A Validated Discrete Element Modeling Approach for Studying Geogrid-Aggregate Reinforcement Mechanisms

Yu Qian[1], Erol Tutumluer[2], M. ASCE, and Hai Huang[3]

[1]Graduate Research Assistant, Department of Civil and Environmental Engineering, University of Illinois at Urbana-Champaign, Urbana, IL, 61801, yuqian1@illinois.edu
[2]Professor and Corresponding Author, Department of Civil and Environmental Engineering, University of Illinois at Urbana-Champaign, Urbana, IL, 61801, 217-333-8637, tutumlue@illinois.edu
[3]Research Assistant Professor, Washington Center for Asphalt Technology, Washington State University, Pullman, WA 99164, hai.huang@wsu.edu

ABSTRACT

Geogrids are commonly used in transportation applications for stabilization and reinforcement purposes. Factors affecting the interactions or interlock mechanisms between geogrids and aggregates may include but not limited to aggregate size and shape properties, geogrid types and properties, compactive efforts during installation, and loading conditions. To better quantify these effects, our recent research efforts at the University of Illinois have introduced the use of an image-aided Discrete Element Modeling (DEM) approach for studying the interactions of such local effects, i.e., aggregate particles and geogrid properties interacting at the micro-level to produce a "stiffened or reinforced" zone. A recent experimental study was utilized to model and demonstrate the effectiveness of different aperture-sized biaxial geogrids in the reinforcement of ballast aggregates to reduce settlement under cyclic loading. The image-aided 3-D DEM methodology successfully modeled the interactions between the ballast aggregate size and shape properties and the different aperture sized biaxial geogrids. Similar to the experimental study, only certain biaxial geogrid aperture sizes improved the performance of the reinforced ballast when compared to the larger settlement accumulated in the unreinforced ballast. The methodology has the potential for quantifying individual effects of various geogrid products on aggregates with different size and shape properties.

INTRODUCTION

Geogrids, geosynthetic polymeric materials with apertures, are commonly used for the reinforcement objective of granular materials, i.e. aggregates, in the construction of transportation roadways. The main benefit of geogrid is to provide/improve particle interlocking for these granular layers. This has a modest effect on increasing stiffness and a major effect on decreasing particle movement, which in turn affects shear and permanent

deformations. Hence, the right combinations of aggregate and geogrid properties to ensure "good" interlocking must be known.

Although geogrids are known to work quite effectively for providing local stabilization through aggregate interlock, there exists a knowledge gap for adequately identifying and modeling specific mechanisms of micro level interactions between various geogrid types and aggregate particle size and shape properties. For aggregate materials, the properties may include hardness, shape/angularity, shear strength, i.e. friction angle. For geogrids, the properties may include rib/junction strength, aperture size/shape (with respect to particle size/shape, etc.), rib stiffness, shape, and dimension. In addition, the interaction of geogrid with aggregate and the effects of the properties of each material on the overall layered roadway system structural performance need to be investigated and quantified for identifying the interlock mechanisms. Experimental studies on geogrid-reinforced aggregates suggest that an optimum aperture size of the geogrid often exist for a given size of aggregates to maximize the effectiveness of specific geogrid-aggregate reinforcement system (Jewell et al., 1984; Brown et al., 2007). Numerical modeling techniques, such as Discrete Element Modeling (DEM), also show that such an optimum aperture size of the geogrids often exists from three-dimensional DEM type Particle Flow Code (PFC3D) simulations of pull-out tests (Konietzky et al., 2004; McDowell et al., 2006), and two-dimensional Particle Flow Code (PFC2D) simulations of cyclic ramp loading tests (Han and Bhandari, 2009). Note that as opposed to cylindrical or spherical elements used in most commercially available DEM applications, irregular shaped aggregate particles with properties, such as flatness and elongation, angularity, and surface texture, can be quite difficult to quantify individually for a realistic evaluation of the aggregate-geogrid interactions during numerical modeling simulations.

This paper demonstrates the effectiveness of a recently introduced image-aided DEM approach at the University of Illinois for modeling geogrid-aggregate system performances of different aperture sized geogrids (Tutumluer et al., 2007). For this purpose, a recently conducted research study by Brown et al. (2007) has been used to gather results from geogrid–reinforced ballast aggregate box testing. The intent was to control and reduce settlement under dynamic loading and therefore provide the most benefit through optimized selection of geogrid aperture size. The good predictions of the calibrated DEM is intended to validate the applicability of the image-aided DEM methodology for studying geogrid-aggregate interactions and its potential for quantifying individual effects of geogrid aperture size and shape relative to aggregate size and shape, gradation and density, as well as shape and stiffness of ribs and stiffness of junction between ribs of various geogrid products.

AGGREGATE IMAGING BASED DISCRETE ELEMENT MODELING

An image-aided DEM approach has been recently introduced to investigate effects of multi-scale aggregate morphological properties on performances of granular assemblies (Tutumluer et al., 2007). The approach utilizes a DEM program BLOKS3D, which was developed at the University of Illinois originally by Ghaboussi and Barbosa (1990) and enhanced more recently with new, fast contact detection algorithms by Zhao et al. (2006). Imaging technology provides detailed measurement of aggregate shape, texture and angularity properties and has been successfully used in the last two decades for quantifying aggregate

morphology. Among the various particle morphological indices, the flat and elongated (F&E) ratio, the angularity index (AI), and the surface texture (ST) index, all developed using University of Illinois Aggregate Image Analyzer (UIAIA), are key indices (Tutumluer et al., 2002; Rao et al., 2002; Pan and Tutumluer, 2007). Using the image-aided 3-D DEM approach, Tutumluer et al. (2009) successfully demonstrated the potential for studying the interactions of such local effects, i.e., aggregate particles and geogrid properties for mechanical interactions at the micro-level to produce a "stiffened or reinforced" zone.

This paper primarily focuses on validating the image-aided BLOKS3D DEM approach (Tutumluer et al., 2007). For this purpose, a recently conducted University of Nottingham research study (Brown et al., 2007) generated useful information about geogrid-aggregate interaction in the context of railway ballast reinforcement to reduce accumulated settlement due to cyclic loading. Brown et al. (2007) utilized their laboratory full-scale Railway Test Facility to build and test a series of layered railroad track substructures as box setups including both unreinforced and geogrid–reinforced aggregate ballast layers in their experiments. Extruded type biaxial geogrids with varying square aperture sizes were specifically manufactured for the Brown et al. (2007) study to investigate the effectiveness of different aperture sizes in providing the maximum geogrid-aggregate interlock as indicated by the least accumulated settlement under dynamic loading.

The ballast particles from Brown et al. (2007) study were re-generated according to the particle shape properties and gradations and used as discrete elements in the image-aided 3-D DEM approach. The granite type ballast aggregate material was from Glensanda quarry in Scotland. The material can be generally described as uniformly graded, crushed hard stone which is durable, angular, equi-dimensional in shape and relatively non flaky (Brown et al., 2007). The particle size distribution of the granite ballast is shown in Figure 1.

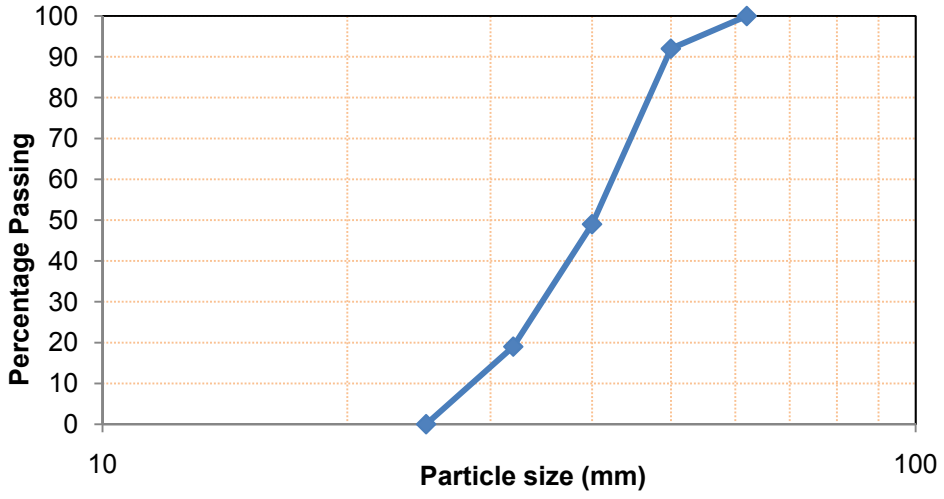

Figure 1. Gradation properties of granite ballast tested by Brown et al. (2007)

Figure 2 presents the aggregate imaging based DEM methodology using the UIAIA for creating 3-D polyhedron shaped representative DEM elements from two 2-D images of an actual aggregate particle. The angularity indices (AI) of the typical crushed granite particles ranged from 500 to 650; the rough textured particles were represented with Surface Texture

(ST) indices ranged from 1.8 to 2.9; and the non-flaky, cubical particles were characterized with flat and elongated (F&E) ratios less than 3 in the DEM simulations for an accurate modeling of the average shape properties in the granular ballast assembly (Tutumluer et al., 2002; Rao et al., 2002; Pan and Tutumluer, 2007). A total of 3,791 aggregate particles were used to model the ballast layer of approximately 300-mm thickness beneath the loading platen.

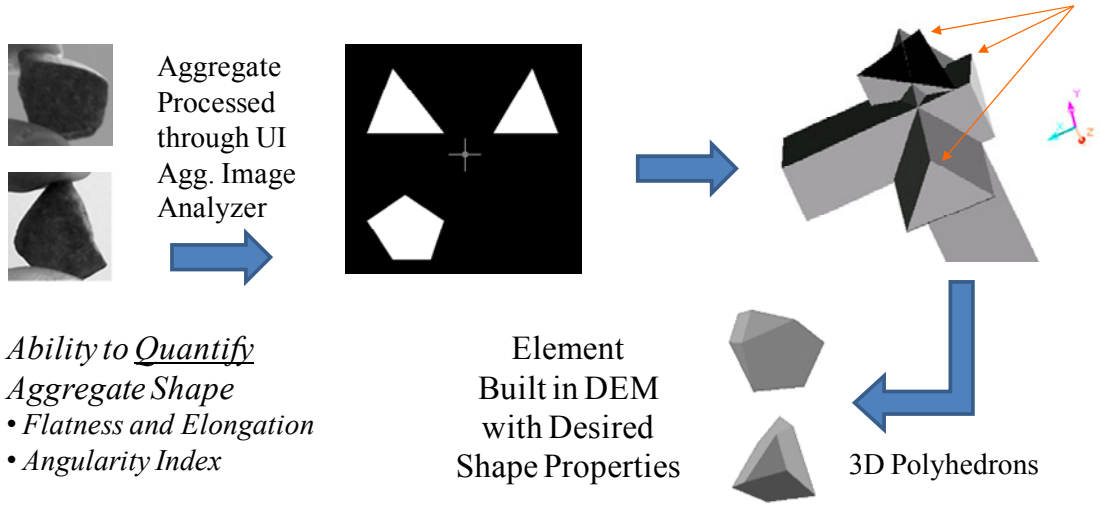

Figure 2. Discrete elements generated from aggregate imaging based DEM methodology

A 14-mm thick rubber sheet with elastic modulus of 30 MPa was generated in DEM to simulate the condition of soft subgrade found at the bottom of the test box by Brown et al. (2007). Above the rubber sheet, the 300-mm thick ballast layer was placed to have a natural slope according to angle of repose from the center of the test box to the sides. To compare different geogrid aperture sizes and evaluate interlocking and local reinforcement effectiveness, all the geogrids created in the DEM simulations were assigned with the same nominal tensile strength of 30 kN/m. The geogrid square openings or aperture sizes studied were 32 mm, 50 mm, 65 mm, and 100 mm in accordance with the experimental study by Brown et al. (2007). Figure 3 shows the typical biaxial geogrid sheet with apertures created for use in DEM simulations. The geogrid was placed at approximately 250 mm depth from the top of the 300-mm thick ballast layer following the box setup by Brown et al. (2007). Figure 4 shows the details of DEM elements used to create the 65-mm aperture single unit biaxial geogrid having a rib cross section 4.2 mm wide and 1.5 mm high.

A visualization overview of the DEM simulations is given in Figure 5. Following the experimental study by Brown et al. (2007), a 20-kN cyclic load was applied in the DEM simulations on a rectangular loading platen/beam, 0.7 m long and 0.25 m wide. This loading applied approximately a uniform pressure of 114 kPa on the ballast layer. The load pulse used in the DEM simulations consisted of a sine wave with the equivalent frequency of 2 Hz.

The responses of both unreinforced and geogrid-reinforced ballast test sections were investigated according to the experiments conducted by Brown et al. (2007). At this stage, several runs of the 3-D DEM simulations were conducted to investigate the influences of four different geogrid aperture sizes on the local reinforcement effectiveness and hence reductions

in the predicted ballast permanent deformations under cyclic loading when compared to the unreinforced case. In addition, to adequately identify the level of geogrid-aggregate interlocking and the local "stiffening or reinforcement" effectiveness of the geogrid, the results from with and without geogrid cases are also compared by means of the DEM predicted contact forces in the ballast layer (Tutumluer et al., 2009).

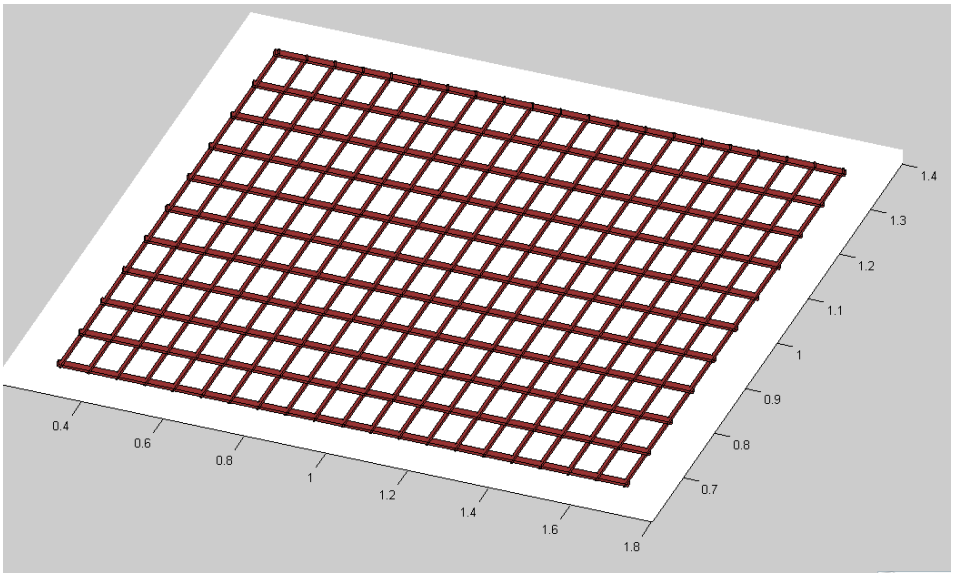

Figure 3. Typical biaxial geogrid sheet used in DEM simulations

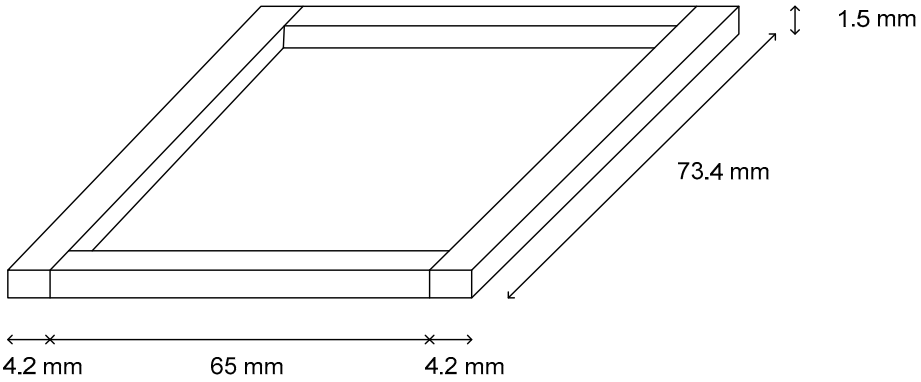

Figure 4. Details of DEM elements for the 65-mm aperture single unit biaxial geogrid

DEM SIMULATION RESULTS AND DISCUSSION

Due to the long DEM run times associated with each loading case, the DEM simulations for the settlement or permanent deformation predictions considered only up to 40 cycles of the load application. Because of the significantly high number of aggregate particle contact forces computed and checked for global granular assembly equilibrium at each

iterative time step, a relatively low number of initial load cycles, such as 40 achieved here for several different simulation cases studied, was deemed to be sufficient for identifying the main reinforcement mechanisms and interlocking trends in this situation.

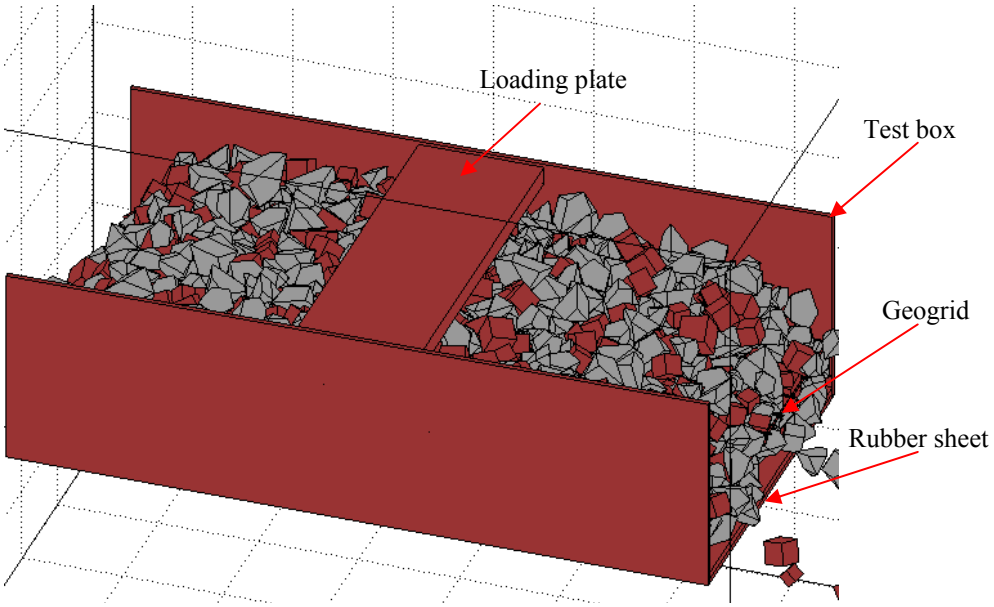

Figure 5. DEM simulation overview of the laboratory test setup by Brown et al. (2007)

To validate the DEM approach and in the meantime to study for the optimum aperture size of geogrids matching with aggregate particle sizes and shapes, numerical simulations were prepared for different initial conditions. Ballast was compacted to different levels with void ratios ranging from 38% to 45%. For the loosely compacted ballast layer (void ratio = 45%), quite large deformations were obtained for both the unreinforced and geogrid-reinforced cases.

At an initial void ratio of 38%, both the unreinforced and the 65-mm aperture sized geogrid-reinforced case displacement measurements from the experimental study (Brown et al. 2007) could be predicted reasonably accurately from the DEM simulations (see Figure 6). Note that for a well-compacted ballast layer, geogrid cannot be properly mobilized at a load cycle of 40 since the deformation would be very small, which was also shown in the experimental study findings (Brown et al. 2007). Although the geogrid-reinforced case indicates lower displacements, there is simply not a significant difference in the performances of the unreinforced and geogrid-reinforced cases within the relatively low number of initial load cycles as shown in Figure 6.

Figure 7 presents the permanent deformation trends predicted with the number of load cycles for both the unreinforced case and the reinforced ballast layers with geogrids having aperture sizes of 50 mm, 65 mm and 100 mm. Although the permanent deformations predicted are similar initially, they differ in the accumulation trends as reported by Brown et al. (2007). With the number of load cycles increasing beyond 5, the reinforcement benefit of geogrid becomes more apparent. Geogrids with different aperture sizes have quite different settlements

resulting from the changes in local stiffening and aggregate interlock; the 65-mm aperture size gave the lowest predicted displacements. Similar to the experimental findings by Brown et al. (2007), the geogrid aperture size is strongly related to the size and shape properties of aggregates; there is an optimum geogrid aperture size in relation to the ballast size and shape properties for maximizing the effectiveness of reinforcement. In this study, the 65-mm aperture size was found to be optimum for the average aggregate size, D_{50}, of 40 mm.

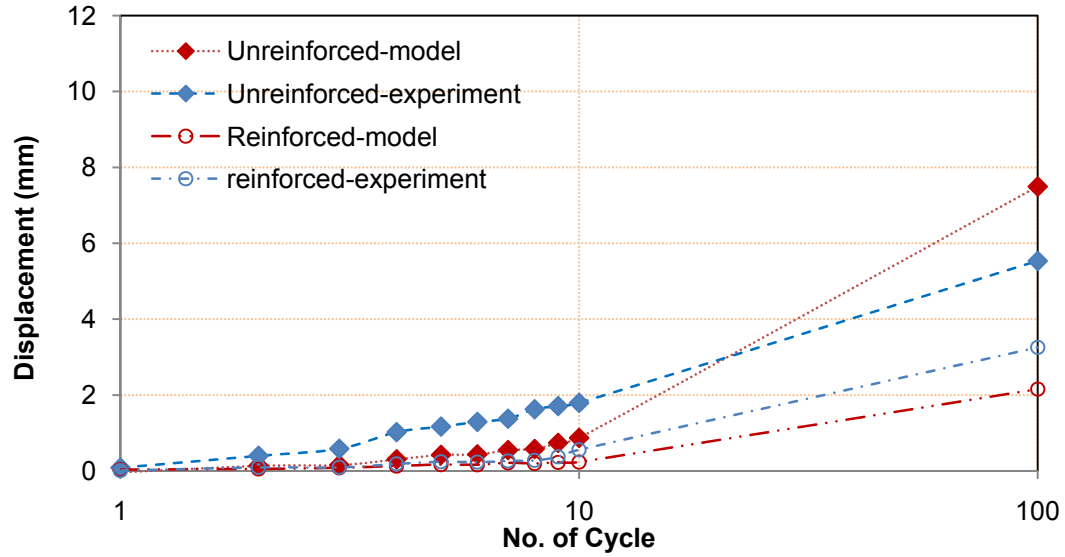

Figure 6. Predicted permanent deformations from well-compacted initial condition (void ratio = 0.38) compared with experimental (Brown et al. 2007) results

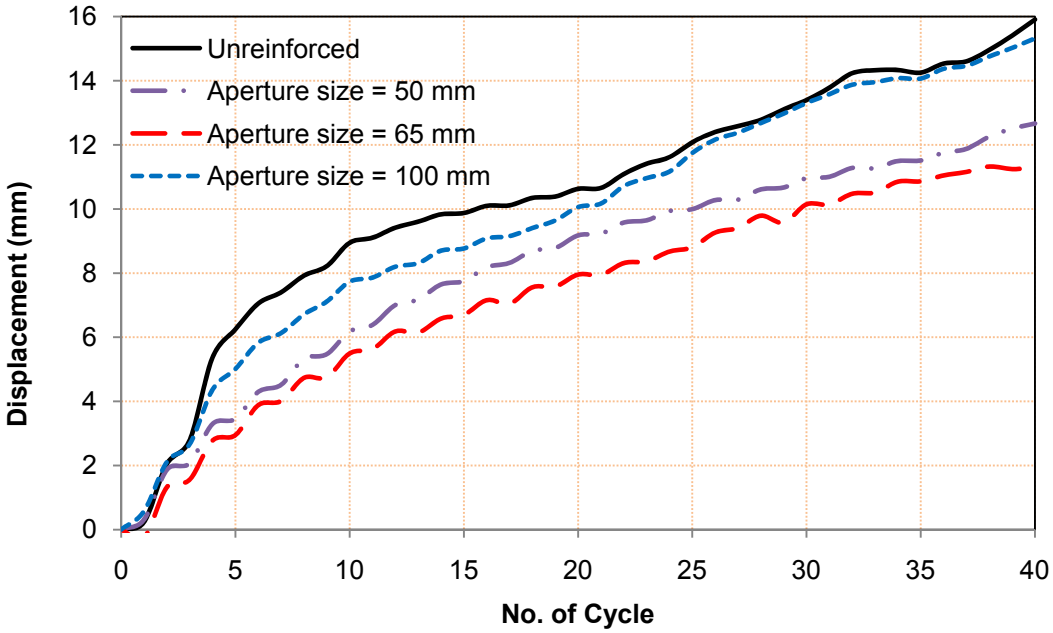

Figure 7. Predicted permanent deformations or settlements with load cycles

Figure 8 presents the predicted permanent deformations at the 40th cycle for both the unreinforced case and the geogrid reinforced ballast layers. The values are 15.9 mm for the unreinforced case and 12.7 mm, 11.3 mm, and 15.3 mm for the reinforced cases with geogrid aperture sizes of 50 mm, 65 mm and 100 mm, respectively. Clearly, the unreinforced case yields a similar displacement to that of the geogrid reinforcement with the 100-mm aperture size. In other words, considering the ballast aggregate size distribution given in Figure 1, the 100-mm geogrid aperture opening was quite large for any significant geogrid-aggregate interlocking to take place. However, the geogrid with the 50-mm aperture size provided considerable improvement; and, the geogrid with the 65-mm aperture size had the most significant improvement yielding the lowest displacement (see Figure 8). This is in accordance with the experimental results reported in the University of Nottingham study (Brown et al., 2007). Therefore, these good predictions validate the applicability of the introduced aggregate imaging based DEM approach for studying geogrid-aggregate reinforcement mechanisms.

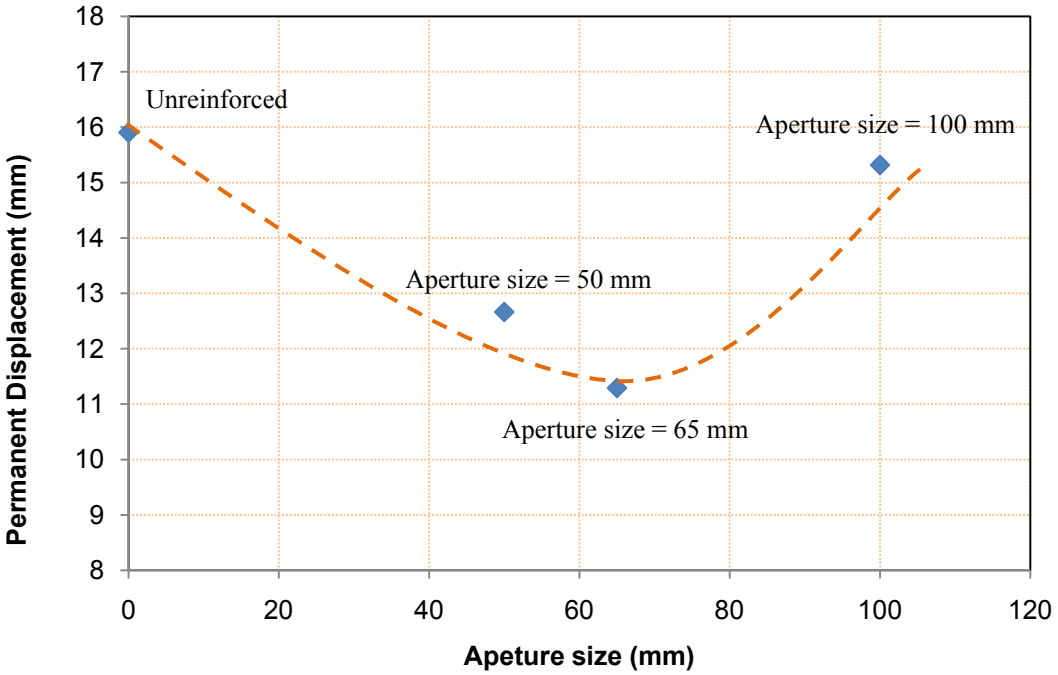

Figure 8. Permanent displacements predicted from DEM approach at the 40th load cycle

Figure 9 presents the ballast aggregate particle contact force distributions obtained as vector plots at the 40th load cycle for the unreinforced case and for the ballast layer reinforced with the 65-mm aperture geogrid, respectively. Note that in the unreinforced case, the forces among the aggregate particles are relatively small and somewhat evenly distributed with depth. For the reinforced case with the 65-mm aperture geogrid, the contact forces are much higher in magnitude and concentrated in the lower part of the test box, where approximately the geogrid was placed. This location of the geogrid can be referred to as the "stiffened or reinforced" zone due to the significant interaction of geogrid and aggregates.

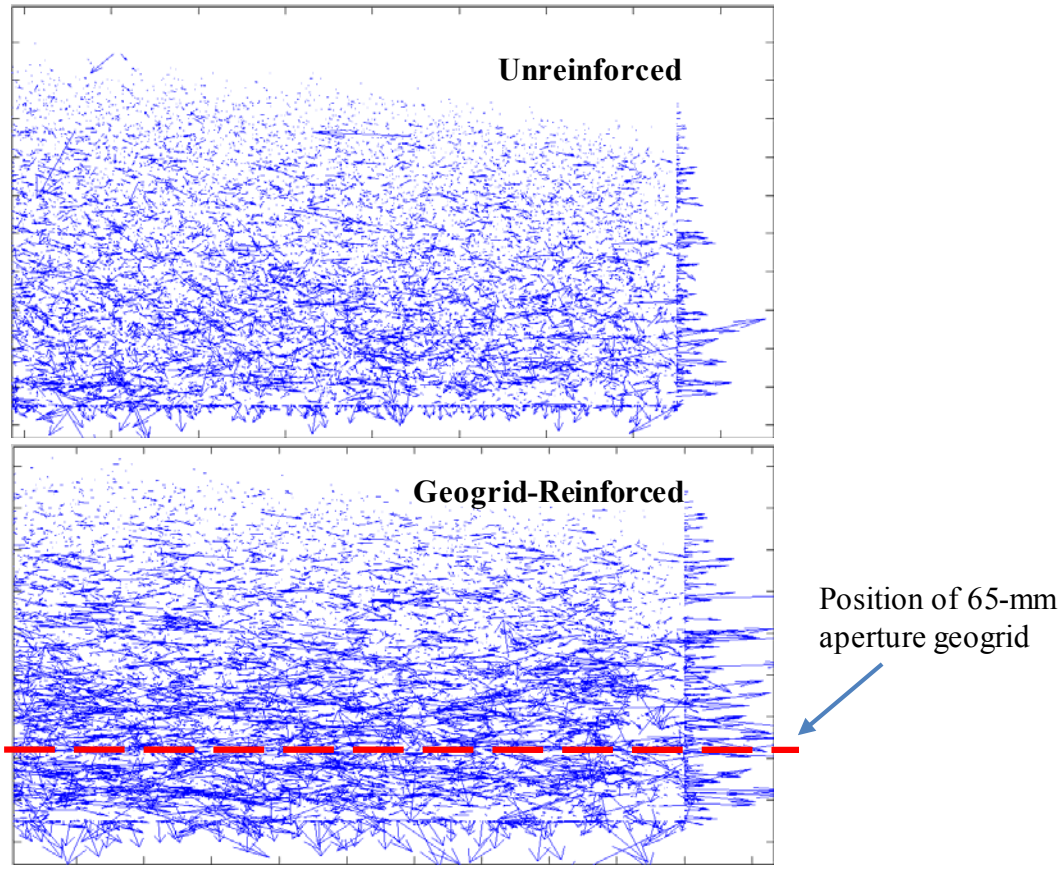

Figure 10. Contact forces predicted by DEM simulation at the 40th load cycle

CONCLUSIONS

This paper demonstrated the applicability of an aggregate particle imaging based three-dimensional (3-D) Discrete Element Modeling (DEM) approach for studying geogrid-aggregate reinforcement mechanisms. For this purpose, a recent experimental study was utilized to model the effectiveness of different aperture-sized biaxial geogrids in the reinforcement of ballast aggregates to reduce settlement under cyclic loading. The following conclusions can be drawn from this study:

1. The image-aided DEM approach was used to successfully generate discrete elements as individual aggregate particles with the actual size distribution (gradation) and shape properties, such as flatness, elongation, texture and angularity.
2. Similar to the experimental study, only certain biaxial geogrid aperture sizes improved the performance of the reinforced ballast when compared to the larger settlement accumulated in the unreinforced ballast. The geogrid with the 65-mm aperture size had the most significant improvement from DEM simulations yielding the lowest ballast settlement for the average ballast aggregate size, D_{50}, of 40 mm.
3. Higher magnitude aggregate particle contact force distributions predicted in the geogrid-

reinforced ballast layer after 40 load cycles clearly indicated a "stiffened or reinforced" zone due to the significant interaction of the geogrid ribs and the aggregate particles. The improved performance of the geogrid-reinforced ballast depends on this interaction between geogrids and aggregate particles.

4. The image-aided 3-D DEM methodology successfully modeled the interactions between the ballast aggregate size and shape properties and the different aperture sized biaxial geogrids. The methodology has the potential for quantifying individual effects of various geogrid products to aggregates with different sizes and shape, gradation and density.

REFERENCES

Brown, S. F., Kwan, J., and Thom, N. H. (2007). "Identifying the Key Parameters That Influence Geogrid Reinforcement of Railway Ballast*." Geotextiles and Geomembranes* Vol. 25, pp. 326-335.

Ghaboussi, J and Barbosa, R. (1990). "Three-dimensional Discrete Element Method for Granular Materials," *International Journal for Numerical and Analytical Methods in Geomechanics,* Vol. 14, pp. 451-72.

Han, J. and Bhandari, A. (2010). "The Influence of Geogrid Aperture Size on the Behavior of the Reinforced Granular Bases" Proceedings of International Symposium on Geomechanics and Geotechnics, October 10-12, 2010, Shanghai, China.

Jewell, R.A., Milligan, G.W.E., Sarsby, R.W. and Dubois, D. (1984). "Interaction Between Soil and Geogrids," Proceedings Symposium on Polymer Grid Reinforcement in Civil Engineering, London, U.K., pp. 19-29.

Konietzky, H., te Kamp, L., Gröger, T. and Jenner, C. (2004). "Use of DEM to Model the Interlocking Effect of Geogrids under Static and Cyclic Loading," *Numerical Modeling in Micromechanics via Particle Methods*: Shimizu, Y., Hart, R. & Cundall, P. (Eds.), A.A. Balkema, Rotterdam, pp. 3-12.

McDowell, G., R., Harireche, O., Konietzky, H., Brown, S. F., Kwan, J., and Thom, N. H. (2006). "Discrete Element Modeling of Geogrid-Reinforced Aggregates," *Geotechnical Engineering* Vol. 159, pp. 35-48.

Tutumluer, E., Huang, H., Hashash, Y. M. A., and Gaboussi, J. (2007). "Discrete Element Modeling of Railroad Ballast Settlement," Proceedings of 2007 AREMA Annual Conference, Chicago, Illinois, September, 9-12, 2007.

Tutumluer, E., Huang, H., Bian, X. (2009). "Research on the Behavior of Geogrids in Stabilisation Applications." Jubilee Symposium on Polymer Geogrid Reinforcement Conference, London, UK, September 8, 2009.

Zhao D., Nezami, E. G., Hashash, Y. H.A., and Gaboussi, J. (2006). "Three-Dimensional Discrete Element Simulation for Granular Materials," *Journal of Engineering Computations,* Vol. 23, No. 7, pp. 749-770.

Pan, T. and Tutumluer, E. (2007). "Quantification of Coarse Aggregate Surface Texture Using Image Analysis," *ASTM Journal of Testing and Evaluation*, Vol. 35, Issue 2, March.

Rao, C., Tutumluer, E. and Kim, I.T. (2002). "Quantification of Coarse Aggregate Angularity Based on Image Analysis," *Transportation Research Record. No. 1787*, TRB, National Research Council, Washington, DC, pp. 193-201.